# Effect of Hydrogen Bonding on the Physicochemical Properties and Bilayer Self-Assembly Formation of *N*-(2-Hydroxydodecyl)-L-alanine in Aqueous Solution

Arjun Ghosh and Joykrishna Dey*

*Department of Chemistry, Indian Institute of Technology, Kharagpur−721 302, India*

*Received January 23, 2008. Revised Manuscript Received March 6, 2008*

The aggregation behavior of *N*-(2-hydroxydodecyl)-L-alanine ($C_{12}$HAla) and *N*-(*n*-dodecyl)-L-alanine ($C_{12}$Ala) was studied in aqueous buffer (pH 12) over a concentration range above their critical aggregation concentration (cac). The $C_{12}$HAla amphiphile has two cacs in contrast to only one cac value for $C_{12}$Ala. The micropolarity and microviscosity of the aggregates were studied by use of pyrene and 1,6-diphenyl-1,3,5-hexatriene, respectively, as fluorescent probes. Dynamic light scattering was used to measure the average hydrodynamic diameter and size distribution of the aggregates. Large size, high microviscosity, and low micropolarity values of the aggregates suggested the formation of bilayer structures in dilute solutions of $C_{12}$HAla. In contrast, $C_{12}$Ala was observed to form micelles. Transmission electron micrographs of dilute and moderately concentrated solutions of $C_{12}$HAla revealed the existence of spherical vesicles and branching tubular structures, respectively. Comparison of the aggregation behavior of these amphiphiles to that of $C_{12}$Ala and the FT-IR spectrum suggested that intermolecular hydrogen-bonding interactions between adjacent hydrocarbon chains through the -OH and -NH- groups of $C_{12}$HAla are responsible for bilayer formation. The mechanism of nanotube formation was discussed. The temperature dependence of aggregate formation of the amphiphile also was investigated.

## Introduction

Recent studies have shown that short-range attractive interactions, such as hydrogen bonding, could be a driving force in the formation of bilayer self-assemblies of single-chain surfactants.[1–6] In fact, hydrogen bonding between the amide groups is responsible for the favorable aggregation of some cationic surfactants that carry amide group spacers between the hydrophobic tail and the quaternary ammonium ion.[7–10] We also have shown that intermolecular hydrogen bonding (IHB) between secondary amide groups in the hydrophobic tail of sodium 11-acrylamidoundecanoate[1] induces a stable linear state. Others also have reported IHB interactions of the amide group bonded to the chiral carbon of *N*-acylamino acid surfactants in Langmuir−Blodgett monolayers (LBM).[11,12] More recently, we investigated the aggregation behavior of a series of sodium salts of *N*-(11-acrylamidoundecanoyl)-L-amino acids[13–15] and *N*-(4-*n*-alkyloxybenzoyl)-L-amino acids[16–18] in water. The IHBs between amide groups of hydrophobic chains and headgroups were shown to be responsible for bilayer formation. It is well-known that hydrogen bonds play very important roles in biological systems. Hydrogen bonds have a directional property and are moderately strong (4−25 kJ $mol^{-1}$).[19,20] One of the important features of hydrogen bonding is that the bond formation can be reversibly switched under mild conditions by physical stimuli such as heat. In fact, hydrogen bonds have become a tool in liquid crystal (LC)[21,22] and polymer[23,24] chemistry. The role of hydrogen bonding on the gelation of organic solvents and water is well-documented in the literature.[25] Hidaka et al. reported the gelation of organic solvents by *N*-(2-hydroxydodecyl)-α-amino acids.[26] It has been demonstrated that these amphiphilic molecules exist in fibrous helical aggregates in organic solvents. Some of these compounds containing a hydroxyl group and an asymmetric carbon atom also have thermotropic liquid crystalline properties in which the -OH group in the alkyl chain plays an important role by enabling

* Corresponding author. Tel.: 91-3222-283308; fax: 91-3222-255303; e-mail: joydey@chem.iitkgp.ernet.in.

(1) (a) Roy, S.; Dey, J. *Langmuir* **2003**, *19*, 9625–9629. (b) Khatua, D.; Dey, J. *J. Phys. Chem. B* **2007**, *111*, 124–130. (c) Ohta, A.; Tani-I, K.; Hoshiba, A.; Asakawa, T.; Miyagishi, S. *Chem. Lett.* **2005**, *34*, 560–561.

(2) Sakamoto, K.; Hatano, M. *Bull. Chem. Soc. Jpn.* **1980**, *53*, 339–343.

(3) Shinitzky, M.; Haimovitz, R. *J. Am. Chem. Soc.* **1993**, *115*, 12545–12549.

(4) (a) Du, X.; Hlady, V. *J. Phys. Chem. B* **2002**, *106*, 7295–7299. (b) Bhattacharya, S.; Krishnan-Ghosh, Y. *Chem. Commun. (Cambridge, U.K.)* **2001**, 185–186. (c) Luo, X.; Liu, B.; Liang, Y. *Chem. Commun. (Cambridge, U.K.)* **2001**, 1556–1557. (d) Boetcher, C.; Schade, B.; Fuhrhop, J.-H. *Langmuir* **2001**, *17*, 873–877.

(5) Imae, T.; Takahasshi, Y.; Muramatsu, H. *J. Am. Chem. Soc.* **1992**, *114*, 3414–3419.

(6) Roy, S.; Khatua, D.; Dey, J. *J. Colloid Interface Sci.* **2005**, *292*, 255–264.

(7) Pires, P. A. R.; El Seoud, O. A. *Prog. Colloid Polym. Sci.* **2006**, *133*, 131–141.

(8) Shimizu, S.; Pires, P. A. R.; Fish, H. K.; Halstead, T. K.; El Seoud, O. A. *Phys. Chem. Chem. Phys.* **2003**, *5*, 3489–3497.

(9) Shimizu, S.; Pires, P. A. R.; El Seoud, O. A. *Langmuir* **2003**, *19*, 9645–9652.

(10) Shimizu, S.; El Seoud, O. A. *Langmuir* **2003**, *19*, 238–243.

(11) (a) Du, X.; Liang, Y. *J. Phys. Chem. B* **2001**, *105*, 6092–6060. (b) Du, X.; Liang, Y. *J. Phys. Chem. B* **2000**, *104*, 10047–10100. (c) Du, X.; Liang, Y. *Langmuir* **2000**, *16*, 3422–3434.

(12) Du, X.; Hlady, V. *J. Phys. Chem. B* **2002**, *106*, 7295–7299, and references therein.

(13) Roy, S.; Dey, J. *Langmuir* **2005**, *21*, 10362–10369.

(14) Roy, S.; Dey, J. *Bull. Chem. Soc. Jpn.* **2006**, *79*, 59–66.

(15) Roy, S.; Dey, J. *J. Colloid Interface Sci.* **2007**, *307*, 229–234.

(16) Mohanty, A.; Dey, J. *Langmuir* **2004**, *20*, 8452–8459.

(17) Mohanty, A.; Dey, J. *Langmuir* **2007**, *23*, 1033–1040.

(18) Mohanty, A.; Patra, T.; Dey, J. *J. Phys. Chem. B* **2007**, *111*, 7155–7159.

(19) Jeffy, G. A. *An Introduction to Hydrogen Bonding*; Oxford University Press: New York, 1997; pp 253−256.

(20) MacDonald, J. C.; Whitesides, G. M. *Chem. Rev.* **1994**, *94*, 2383–2420.

(21) Kato, T.; Frechet, J. M. J. *Macromolecules* **1989**, *22*, 3818–3819.

(22) Peleos, C. M.; Tsiourvas, D. *Angew. Chem., Int. Ed. Engl.* **1995**, *34*, 1696–1711.

(23) Lange, R. F. M.; van Gurp, M.; Meijer, E. W. *J. Polym. Sci., Part A: Polym. Chem.* **1999**, *37*, 3657–3670.

(24) (a) Bladon, P.; Griffin, A. C. *Macromolecules* **1993**, *26*, 6604–6410. (b) Lutz, J.-F.; Pfeifer, S.; Chanana, M.; Thünemann, A. F.; Bienert, R. *Langmuir* **2006**, *22*, 7411–7415.

(25) (a) Estoff, L. A.; Hamilton, A. D. *Chem. Rev.* **2004**, *104*, 1201–1217. (b) Khatua, D.; Maity, R.; Dey, J. *Chem. Commun. (Cambridge, U.K.)* **2006**, 4903–4905, and references therein.

(26) Hidaka, H.; Murata, M.; Onai, T. *Chem. Commun. (Cambridge, U.K.)* **1984**, 562–564.

10.1021/la800232x CCC: $40.75 
Published on Web 05/16/2008

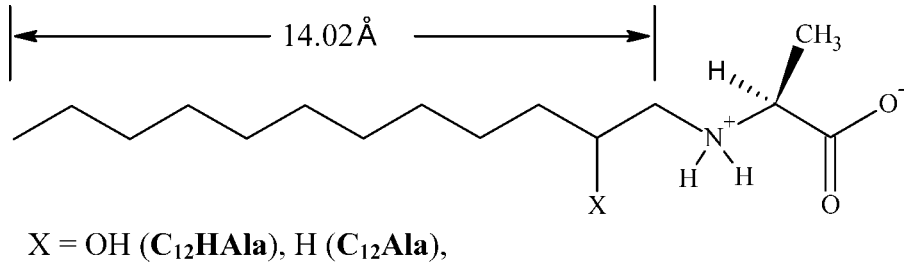


**Figure 1.** Structure of *N*-(2-hydroxy-*n*-dodecyl)-L-alanine ($C_{12}$HAla) and *N*-(*n*-dodecyl)-L-alanine ($C_{12}$Ala).

formation of intermolecular hydrogen bonds.[27] LBM studies at the air−water interface have suggested that OH-substitution near (2- or 3-position) the headgroup results in a loss of ordering, which is caused by headgroup enlargement by the neighboring -OH group and a misfit of the alkyl chains in hydroxypalmitic acid.[28] On the other hand, well-shaped condensed phase domains were found after the phase transition in 9-hydroxypalmitic acid, in which the -OH group is near the center of the hydrocarbon chain. The stability of the LC phase formed by the fatty acid derivatives bearing the -OH group is influenced by the ability of the substituent to form IHBs and cause little disorder in the packing of the alkyl chain. The hydrogen-bonding role of the -OH group in molecular cohesion in a condensed monolayer, helical ribbon, and gel formation by 12-hydroxyoctadecanoic acid has been reported by Tachibana and co-workers.[29] This attracted our attention toward self-assembly properties of the amino acid-derived amphiphiles containing a -OH group in the alkyl chain.

Chirality of amphiphilic molecules also was observed to have an important effect on the shape of self-assembled supramolecular aggregates.[30,31] Many chiral amphiphilic molecules form long, narrow tubules instead of flat bilayers, although the latter is normally expected to be the lowest energy state of bilayer aggregates.[32,33]

Zhang and co-workers[34] reported branching nanotube formation in aqueous dispersions of peptide surfactants. The roles of hydrogen bonding in the formation of nanotubes, nanovesicles, and gels by surfactant-like peptides were demonstrated by Paramonov et al.[35] On the other hand, Ghadiri and co-workers[36] demonstrated the formation of self-assembling nanotubes of alternating D,L-α-peptides and cyclic $\beta$-peptides. According to these authors, the monomeric peptide units first form segments of a bilayer ring, which grows into single subunit rings and multirings. The tubular arrays then stack through backbone−backbone hydrogen-bonding interactions to form longer nanotubes. Recent developments of peptide nanotubes[37–39] have found many applications.[40–44]

It is well-known that the spontaneous curvature of a surfactant aggregate is related to the relative sizes of the hydrophilic head and hydrophobic tail of the surfactant molecule. An increase of attractive forces between the headgroups can cause a decrease in effective headgroup area and hence a decrease in the curvature of the aggregate. In other words, this is a driving force for aggregate growth. Our recent work on *N*-(2-hydroxydodecyl)-L-valine ($C_{12}$HVal) has shown that the amphiphile forms branching nanotubes in aqueous medium.[45] Although the possible role of hydrogen-bonding interactions through the chain -OH group was implicated in this report, no clear evidence was given for this. The questions we address in this report are (i) can the hydrogen-bonding effect of the -OH group change the shape of the aggregate and (ii) can this hydrogen-bonding interaction give rise to significant aggregate growth at low concentrations? Thus, to investigate the role of the -OH group in the alkyl chain of the surfactant on nanotube formation, we undertook this study of self-assembly properties and shapes of the aggregates that are formed by such surfactants. For this study, we synthesized two *N*-alkyl amino acids: *N*-(2-hydroxydodecyl)-L-alanine ($C_{12}$HAla) and *N*-(*n*-dodecyl)-L-alanine ($C_{12}$Ala) (see Figure 1 for molecular structures). The investigations were performed using various techniques such as surface tension, conductivity, fluorescence, dynamic light scattering, transmission electron microscopy (TEM), and FT-IR spectroscopy. The data obtained from different experiments were used to gain information about the solution structure of the self-assemblies formed by the surfactants.

## Experimental Procedures

**Materials.** *N*-(2-Hydroxy-*n*-dodecyl)-L-alanine ($C_{12}$HAla) was prepared from L-alanine and 1,2-epoxydodecane according to a procedure described elsewhere.[26] The product was purified by recrystallization from ethanol or an ethanol−water mixture. Since the 1,2-epoxydodecane employed was racemic, we obtained only the racemic (with respect to the hydroxylic carbon) compound. Details of synthesis and chemical identification are given in the Supporting Information. On the other hand, *N*-(*n*-dodecyl)-L-alanine ($C_{12}$Ala) was synthesized from the reaction of 1-bromo-dodecane and L-alanine.[46] 1,2-Epoxydodecane and 1-bromododecane were purchased from Aldrich (Milwaukee, WI). L-Alanine was purchased

(27) Ueda, T.; Hidaka, H.; Harada, H.; Yamashita, Y.; Ohkura, A. *Mol. Cryst. Liq. Cryst.* **1982**, *84*, 231–243.
(28) Siegel, S.; Vollhardt, D.; Cadenhead, D. A. *Colloids Surf., A* **2005**, *256*, 9–15, and references therein.
(29) (a) Tachibana, T.; Yoshizumi, T.; Hori, K. *Bull. Chem. Soc. Jpn.* **1979**, *52*, 34–41. (b) Tachibana, T.; Kambara, H. *Bull. Chem. Soc. Jpn.* **1969**, *42*, 3422–3424.
(30) Zhang, L.; Lu, Q.; Liu, M. *J. Phys. Chem. B* **2003**, *107*, 2565–2569.
(31) Yuan, J.; Liu, M. *J. Am. Chem. Soc.* **2003**, *125*, 5051–5056.
(32) Blanzat, M.; Massip, S.; Spéziale, V.; Perez, E.; Rico-Lattes, I. *Langmuir* **2001**, *17*, 3512–3514.
(33) Fuhrhop, J.-H.; Helfrich, W. *Chem. Rev.* **1993**, 1565–1582.
(34) Sylvain, V.; Santoso, S.; Gong, H.; Watson, N.; Zhang, S. *Proc. Natl. Acad. Sci. U.S.A.* **2002**, *99*, 5355–5360.
(35) Paramonov, S. E.; Jun, H. W.; Hartgerink, J. D. *J. Am. Chem. Soc.* **2006**, *128*, 7291–7298.
(36) (a) Bong, D. T.; Clark, T. D.; Granja, J. R.; Ghadiri, M. R. *Angew. Chem., Int. Ed.* **2001**, *40*, 988–1011. (b) Fernandez-Lopez, S.; Kim, H. S.; Choi, E. C.; Delgado, M.; Granja, J. R.; Khasanov, A.; Kraehenbuehl, K.; Long, G.; Weinberger, D. A.; Wilcoxen, K. M.; Gghadiri, M. R. *Nature (London, U.K.)* **2001**, *41*, 452–455.
(37) Matsui, H.; Gologan, B. *J. Phys. Chem. B* **2000**, *104*, 3383–3386.
(38) Matsui, H.; Douberly, G. E. *Langmuir* **2001**, *17*, 7918–7922.
(39) Kogiso, M.; Ohnishi, S.; Yase, K.; Masuda, M.; Shimizu, T. *Langmuir* **1998**, *14*, 4978–4986.
(40) Matsui, H.; Pan, S.; Gologan, B.; Jonas, S. *J. Phys. Chem. B* **2000**, *104*, 9576–9579.
(41) Matsui, H.; Pan, S.; Douberly, G. E. *J. Phys. Chem. B* **2001**, *105*, 1683–1686.
(42) Douberly, G. E.; Pan, S.; Walters, D.; Matsui, H. *J. Phys. Chem. B* **2001**, *105*, 7612–7618.
(43) Matsui, H.; Gologan, B.; Pan, S.; Douberly, G. E. *J. Eur. Phys. D* **2001**, *16*, 403–406.
(44) Matsui, H.; Porrata, P.; Douberly, G. E. *Nano Lett.* **2001**, 461–464.
(45) Ghosh, A.; Dey, J. *J. Phys. Chem. B*, submitted for publication.

from SRL (Mumbai, India) and was used without further purification. The fluorescence probes, *N*-phenyl-1-naphthylamine (NPN), pyrene, and 1,6-diphenyl-1,3,5-hexatriene (DPH), were obtained from Aldrich (Milwaukee, WI) and were purified by repeated recrystallization from an ethanol−acetone mixture. Analytical grade sodium hydroxide and hydrochloric acid were procured locally and were used directly from the bottle. Double distilled water was used for the preparation of aqueous solutions.

**Methods and Instrumentation.** The FT-IR spectra were measured with a PerkinElmer (Model Spectrum Rx I) spectrometer. The $^1$H NMR spectra were measured with a Bruker 200 MHz (Model Avance-200) instrument with TMS as a standard. Melting point measurements were performed using an Instind (Kolkata) melting point apparatus with open capillaries. A Digital pH meter (Model PH 5652, EC India Ltd., Kolkata) was used for pH measurements. Conductivity was measured with a Thermo Orion conductivity meter (model 150 A+) by use of a cell having a cell constant equal to 0.467 cm$^{-1}$. The measurements of optical rotations were performed with a Jasco (Model P-1020) digital polarimeter. All measurements were performed at room temperature (∼30 °C) unless otherwise mentioned.

The surface tension (ST), $\gamma$, measurements were performed with an automated surface tensiometer (Model 3S, GBX) using the Du Nuöy ring detachment method. The temperature was controlled at 30 ± 0.1 °C by use of a Thermo-Neslab RTE-7 circulating bath. The Pt−Ir ring was carefully cleaned with a 50% ethanol−HCl solution and finally with distilled water. The instrument was calibrated and checked by measuring the $\gamma$ of distilled water. Stock solutions of surfactants were made in phosphate buffer. An aliquot of this solution was transferred to a Teflon beaker (cleaned with sulfochromic acid) containing a known volume of buffer. The solution was gently stirred magnetically and allowed to equilibrate for ∼5 min at 30 °C, and then $\gamma$ was measured. For each measurement, at least three readings were taken, and the mean $\gamma$ value was recorded.

The UV−vis spectra were recorded on a Jasco (Model V-530) spectrophotometer. Fluorescence spectra of the pyrene probe (∼2 × 10$^{-7}$ M) were obtained with a SPEX Fluorolog-3 spectrofluorometer. The samples were excited at 335 nm, and the emission spectrum was recorded between 350 and 450 nm. Steady-state fluorescence anisotropy of DPH was measured on a PerkinElmer LS-55 luminescence spectrometer equipped with filter polarizers that use the L-format configuration. The software supplied by the manufacturer automatically determined the correction factor and anisotropy value. In all cases, the anisotropy values were averaged over an integration time of 10 s and a maximum number of five measurements for each sample. The temperature (30 ± 0.1 °C) of the water-jacketed cell holder was controlled by use of a Thermo Neslab RTE-7 circulating bath. Since DPH is insoluble in water, a 0.5 mM stock solution of the probe in methanol was prepared. The final concentration of the probe was adjusted to 1.0 $\mu$M by the addition of an appropriate amount of stock solution. The sample was excited at 350 nm, and the emission intensity was followed at 450 nm using excitation and emission slits with a band-pass of 2.5 and 2.5−7.0 nm, respectively. A 430 nm emission cutoff filter was used to reduce scattered and stray radiation. All fluorescence measurements began 2−3 h after sample preparation.

Time-resolved fluorescence measurements were performed on a time-correlated single-photon counting method that uses a picosecond diode laser at 370 nm (IBH, nanoLED-07) as the light source. The typical response time of this laser system was 70 ps. Fluorescence lifetimes were determined from time-resolved intensity decay by the method of time-correlated single-photon counting. The decays were analyzed using IBH DAS-6 decay analysis software. For all lifetime measurements, the fluorescence decay curves were analyzed by a biexponential or triexponential iterative fitting program provided by IBH.

The dynamic light scattering (DLS) measurements were performed with a Zetasizer Nano ZS (Malvern Instrument Laboratory, Malvern, U.K.) instrument employing a 4 mW He−Ne laser ($\lambda_o$ = 632.8 nm) and a digital correlator. The solution was filtered directly into the scattering cell through a Millipore Millex syringe filter (Triton free, 0.45 $\mu$m). All the scattered photons were collected at a 173° scattering angle at 30 °C. The scattered intensity data were processed using instrumental software to obtain the *z*-average hydrodynamic diameter ($d_H$) and the size distribution of the particles in each sample. Apparent translational diffusion coefficients ($D_{app}$) were calculated by cumulant analysis of the autocorrelation function of the time dependent fluctuation in intensity. The effective hydrodynamic diameter ($d_H$) was estimated from a diffusion coefficient using the Stokes−Einstein equation

$$D_{app} = \frac{k_B T}{3\pi\eta d_H} \quad (1)$$

where $k_B$ is the Boltzmann constant, $T$ is the absolute temperature, and $\eta$ is the viscosity of the solvent.

For TEM measurements, the samples were prepared according to the usual procedure. The surfactant solution was filtered by use of a one-way syringe membrane filter (0.45 $\mu$m). A total of 5 $\mu$L of the surfactant solution was placed on the 400 mesh carbon-coated copper grid, blotted with filter paper, and negatively stained either with freshly prepared 1.5% aqueous uranyl acetate or 1.5% phosphotungstate after adjustment of pH to the solution pH. The specimens were dried overnight in a desiccator before measurement with an electron microscope (JEOL-JEM 2100) operating at 200 kV.

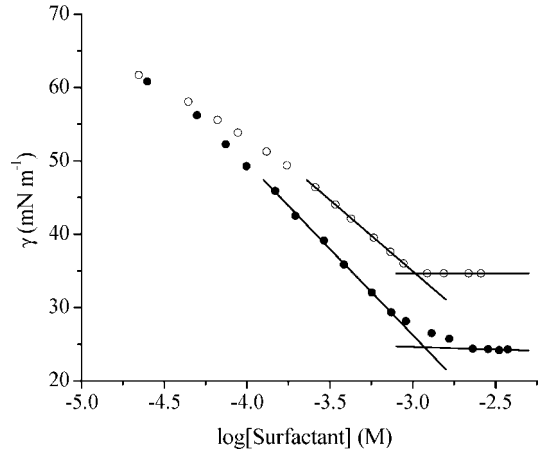


**Figure 2.** Plot of surface tension ($\gamma$) vs log[surfactant]: (●) $C_{12}$HAla and (○) $C_{12}$Ala in 20 mM phosphate buffer (pH 12.0) at 30 °C.

## Results and Discussion

**Ionization Behavior in Solution.** Because the *N*-alkyl amino acids ($C_{12}$HAla and $C_{12}$Ala) are inner salts, their solubility in water is very poor in the pH range of 2−11.5. For $C_{12}$HAla, the p$K_a$ values corresponding to the protonation of -COO$^-$ and dissociation of -NH$_2^+$ groups obtained by a potentiometric titration method (see Figure 1S in the Supporting Information for the titration curve) were found to be 4.0 and 7.8, respectively. Similar values of p$K_a$ also are expected for the $C_{12}$Ala amphiphile. Consequently, the solubility of the amphiphiles increased when the pH was either lowered below 4 or increased above 8. However, a significant aqueous solubility of $C_{12}$HAla and $C_{12}$Ala was observed only at pH ≥ 12. Therefore, to ensure complete deionization of the ammonium group, all solutions were made in phosphate buffer of pH 12.0 for both $C_{12}$HAla and $C_{12}$Ala.

**ST Studies.** The critical aggregation concentration (cac) of the amphiphiles was measured by use of a ST method. The $\gamma$ value decreased with log[surfactant] and showed a break and remained constant thereafter (see Figure 2). The concentration corresponding to the breakpoint (as shown by the intersection

(46) Yoshimura, T.; Visihara, K.; Esumi, K. *Langmuir* **2005**, *21*, 10409–10415.

**Table 1. Self-Assembly Properties of $C_{12}$HAla and $C_{12}$Ala in 20 mM Phosphate Buffer (pH 12) at 30 °C[a]**

| properties | $C_{12}$HAla | $C_{12}$Ala |
|---|---|---|
| cac (mM) | 0.09<br>1.39 (1.18) | 1.04 (1.04) |
| $\gamma_{cac}$ (mN m$^{-1}$) | 24.5 | 34.7 |
| $pC_{20}$ | 3.8 | 4.1 |
| cac/$C_{20}$ | 14.2 | 7.7 |
| $\Gamma_{max} \times 10^6$ (mol m$^{-2}$) | 4.12 | 3.16 |
| $A_m$ (Å$^2$ molecule$^{-1}$) | 40.3 | 52.5 |
| $P$ | 0.66 | 0.48 |
| $I_1/I_3$ | 1.65[b]<br>1.27[c] | 1.05[c] |
| $\eta_m$ (mPa s) | 70.09[c] | 17.18[c] |
| $d_H$ (nm) | 145[b] | 8.0[d] |

[a] cac values within parentheses were obtained from ST measurements. [b] Value indicates the property measured using 0.5 mM surfactant. [c] Value was obtained using 5 mM surfactant. [d] Value was obtained using a surfactant concentration of 20 mM.

of two straight lines) was taken as the cac value. The relevant data are listed in Table 1. The amphiphiles have a relatively low surface tension at the cac ($\gamma_{cac}$), indicating good surface activity. The surface activity parameters, such as cac, surface tension corresponding to cac ($\gamma_{cac}$), and efficiency of adsorption, $pC_{20}$ (negative logarithm of surfactant concentration required to reduce the $\gamma$ value of water by 20 mN/m), were determined from the ST plot in Figure 2. All the physicochemical parameters of $C_{12}$HAla are listed in Table 1. It can be observed that cac and $\gamma_{cac}$ values are lower than the corresponding values of conventional soaps,[47,48] which suggest that both amphiphiles are more surface active than soaps. The same also is indicated by a larger $pC_{20}$ (>3) value.[49] On the other hand, the higher values of the cac/$C_{20}$ ratio indicate that the tendency of the surfactants to adsorb at the air−water interface relative to the formation of aggregates is greater than those of conventional fatty acid salts. It is important to note that the cac and $\gamma_{cac}$ values also are lower than the values of the corresponding sodium salt of *N*-acyl amino acid.[50]

The values of the surface excess ($\Gamma_{max}$) and cross-sectional area per headgroup ($A_{min}$) at the interface were calculated by using the Gibbs adsorption equations[47,49,51]

$$\Gamma_{max} = -\frac{1}{2.303nRT}\frac{d\gamma}{d\log C} \quad (2)$$

$$A_{min} = \frac{1}{N_A\Gamma_{max}} \quad (3)$$

where $d\gamma/d\log C$ is the maximum slope, $N_A$ is Avogadro's number, $T$ is the absolute temperature, $n$ is 1 for a 1:1 ionic surfactant in the presence of a swamping amount of 1:1 electrolyte,[49] and $R$ is 8.314 J mol$^{-1}$ K$^{-1}$. The cross-sectional areas were calculated from $\Gamma_{max}$ values corresponding to the break of the ST plot (Figure 2). $C_{12}$HAla has a lower $A_{min}$ value (Table 1) than that of $C_{12}$Ala and is close to the surface areas of decyl and dodecyl carboxylic acids (45 Å$^2$)[52] at pH 13 in a 0.13 mol kg$^{-1}$ solution. The smaller value of $A_{min}$ in the case of $C_{12}$HAla suggests the formation of large aggregates with tightly packed hydrocarbon chains.

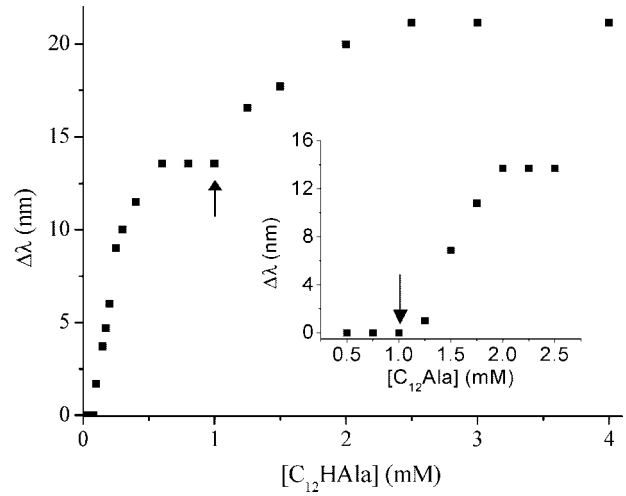


**Figure 3.** Plot of emission wavelength shift ($\Delta\lambda$) of NPN as a function of [$C_{12}$HAla] in 20 mM phosphate buffer (pH 12.0) at 30 °C; inset: plot for $C_{12}$Ala.

**Fluorescence Studies with NPN Probe.** The fluorescent probe, NPN, has been used extensively for the characterization of micellar aggregates.[53] The emission maximum of NPN exhibits a large blue shift accompanied by a huge enhancement of emission intensity relative to that in water upon its incorporation into the hydrophobic environments of micelles.[54] The photophysical properties of NPN are similar to those of 1-anilino-8-naphthalene sulfonic acid (1,8-ANS).[55] Therefore, the steady-state fluorescence spectra of NPN were measured to determine the cac and microenvironments of the aggregates formed by the $C_{12}$Ala and $C_{12}$HAla amphiphiles in water. Figure 3 shows the plots of spectral shifts, $\Delta\lambda$ ($= \lambda_{water} - \lambda_{micelles}$) as a function of surfactant concentration, which were obtained for both amphiphiles. The corresponding plots of relative fluorescence intensity versus surfactant concentration are depicted in Figure 2S in the Supporting Information. It can be observed that unlike $C_{12}$Ala, the plot for $C_{12}$HAla shows two inflections. This is similar to that of $C_{12}$HVal.[45] Thus, the concentrations corresponding to the first (0.09 mM) and second (1.18 mM) inflection can be taken as $cac_1$ and $cac_2$, respectively. The existence of two cac values also was reported for other surfactants.[13–15,56] This suggests that two types of aggregates of different morphologies are formed by $C_{12}$HAla in the concentration range studied. The $cac_2$ value thus obtained is closely similar to the corresponding value obtained from ST measurements. The data in Table 1 suggest that the first cac of $C_{12}$HAla is much lower than the cac value of $C_{12}$Ala. This might be due to higher cohesive forces between the hydrocarbon chains of the former amphiphile. Since the two amphiphiles structurally differ from each other by the presence of a hydroxyl group in the tail, the difference in cac values must be due to the -OH

(47) Pegiadou, S.; Perez, L.; Infante, M. R. *J. Surfactants Deterg.* **2000**, *3*, 517–524.
(48) Ono, D.; Masuyama, A.; Nakatsuji, Y.; Okahara, M.; Yamamara, S.; Takeda, T. *J. Am. Oil Chem. Soc.* **1993**, *70*, 29–36.
(49) Rosen, M. J. *Surfactants and Interfacial Phenomena*, 4th ed.; Wiley-Interscience: New York, 2004.
(50) George, A.; Jain, N.; Desai, A.; Bahadur, P. *Tenside Surfactants Deterg.* **1998**, *35*, 368–374.
(51) Varka, E. M.; Coutouli-Argyropoulou, E.; Infante, M. R.; Pegiadou, S. *J. Surfactants Deterg.* **2004**, *7*, 409–414.
(52) Huang, J-B.; Mao, M.; Zhu, B-Y. *Colloid Surf., A* **1999**, *155*, 339–348.
(53) (a) Félix, M.; Goñi, A. A. *Biochim. Biophys. Acta* **2000**, *1508*, 51–68. (b) Saitoh, T.; Matsushima, S.; Hiraide, M. *Colloids Surf., A* **2007**, *299*, 88–92. (c) Nemkovich, N. A.; Baumann, W.; Kruchenok, Y. V.; Reis, H.; Rubinov, A. N. *J. Fluoresc.* **1997**, *7*, 363–370.
(54) (a) Nayak, R. R.; Roy, S.; Dey, J. *Colloid Polym. Sci.* **2006**, *285*, 219–224. (b) Roy, S.; Nayak, R. R.; Dey, J. *Colloids Surf., A* **2006**, *290*, 62–69.
(55) An extensive compilation of spectral data of 1,8-ANS can be found in a review by Slavic et al. (*Biochim. Biophys Acta* 1982, *694*, 1−25). Since the first excited (S 1) ICT state of the molecule is more stable in water, the gap between S 1 and T 1 states is reduced, thus enhancing the rate of intersystem crossing. Consequently, the molecule is weakly fluorescent in water at longer wavelengths. However, in nonpolar environments, the ICT state is destabilized, thus widening the gap between S 1 and T 1 states. As a result, the fluorescence intensity is enhanced, and the emission band shifts to shorter wavelengths.
(56) (a) Bhattacharya, S.; Haldar, J. *Langmuir* **2004**, *20*, 7940–7947. (b) Won, Y.-Y.; Brannan, A. K.; Davis, H. T.; Bates, F. S. *J. Phys. Chem. B* **2002**, *106*, 3354–3364.

group. The intermolecular hydrogen-bonding interaction between adjacent hydrocarbon chains of the aggregate might be responsible for lowering the cac value. It is also interesting to note that the cac values of the amphiphiles are less than that of sodium *N*-dodecyl-L-alaninate (11.7 mM)[57] in 0.1 N NaOH solution, suggesting that micelle formation is more favored in the case of sodium salts of *N*-alkyl amino acids. However, it should be noted that the Gibbs free energy of formation of micelles depends also upon the shape of the aggregates. In other words, the microstructure formed by these amphiphiles might be different from that of the corresponding sodium *N*-acylamino acid surfactant.

**Micropolarity.** The study of the microenvironmental properties, such as polarity and viscosity, can shed light on the microstructure of the aggregates formed in solution. Also, the change in these properties can give information on structural changes of the aggregates in the system. Fluorescent probes such as NPN, pyrene, and DPH molecules have been used by many authors to investigate microenvironments of surfactant aggregates in solution. It is well-known that the ratio of the intensities of the first and third vibronic bands ($I_1/I_3$) in the fluorescence spectrum of pyrene reflects the polarity of the microenvironment around the probe molecule.[58,59] Therefore, this parameter was used to test changes in the micropolarity induced by water molecules that penetrate by different degrees into this region of the micellar aggregates. The values of the $I_1/I_3$ index for the aggregates formed by the amphiphiles in this study is included in Table 1. The $I_1/I_3$ value for $C_{12}$Ala (1.05) micelles measured at a concentration of 5 times its cac value is much less than that of bulk water (1.76), suggesting that the microenvironment of the pyrene probe molecules is hydrophobic in nature, having a polarity similar to that of 1-pentanol solvent.[58] This means that the probe molecule penetrates more into the hydrophobic core of $C_{12}$Ala micelles. In contrast, the $I_1/I_3$ value (1.65) of $C_{12}$HAla measured at a concentration 5 times its first cac value is slightly less than that of water, indicating that the solubilization site of the probe molecule is hydrophilic and has a polarity equal to that of ethylene glycol solvent.[58] It is also important to note that the $I_1/I_3$ value of $C_{12}$HAla is higher than that of $C_{12}$Ala micelles. This suggests that the pyrene probe is solubilized at the interface of the hydrocarbon core and hydrophilic headgroup region of the micelles of the $C_{12}$HAla amphiphile. However, it is interesting to observe that in the case of $C_{12}$HAla, the value of $I_1/I_3$ decreases (see Figure 4) with the increase of [$C_{12}$HAla]. As can be seen, there is an inflection in the curve (see inset of Figure 4) corresponding to ~1.2 mM $C_{12}$HAla, which is almost equal to the $cac_2$ value obtained from fluorescence probe studies using NPN. This, as discussed earlier, can be attributed to a change in morphology of the aggregates. The $I_1/I_3$ index can be observed to decrease further with an increase of [$C_{12}$HAla] above 1.5 mM, showing another inflection (indicated by the arrow in Figure 4) at ~ 5 mM. This might be associated with the growth of the aggregates with an increase of surfactant concentration. As the aggregates grow, the hydrocarbon chains of the surfactant become tightly packed, and consequently, water molecules are expelled out from the interfacial region of the aggregates, thus decreasing the polarity of the microenvironment of the pyrene molecule. This also means that at relatively higher concentrations, the hydrocarbon chains become less fluid in $C_{12}$HAla micelles as compared to those in $C_{12}$Ala micelles.

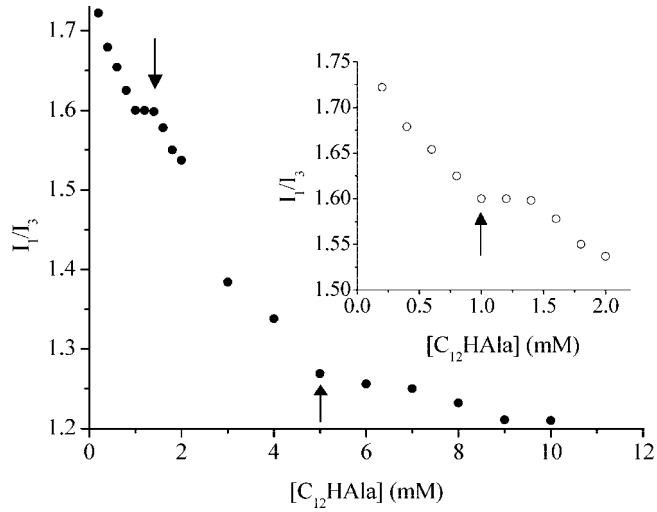


**Figure 4.** Variation of micropolarity parameter ($I_1/I_3$) with [$C_{12}$HAla]. Conditions: 20 mM phosphate buffer, pH 12.0, 30 °C.

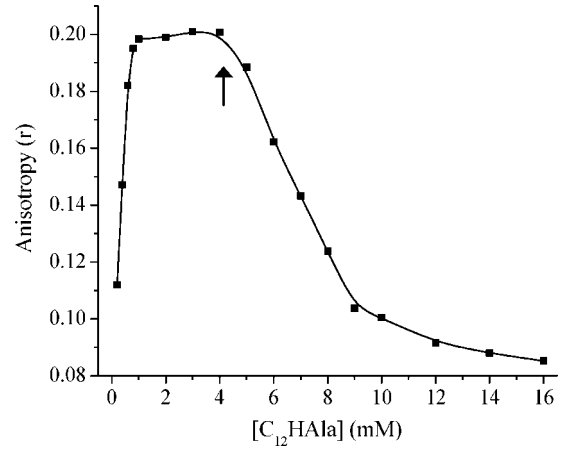


**Figure 5.** Variation of fluorescence anisotropy (*r* value) of the DPH probe with the concentration of $C_{12}$HAla in 20 mM phosphate buffer of pH 12 at 30 °C; the curve is a smoothed line joining the experimental points.

**Microviscosity.** To estimate the microfluidity of the micellar core, we measured the fluorescence anisotropy (*r*) of the DPH probe in the presence of $C_{12}$HAla and $C_{12}$Ala surfactants above their cac values. DPH is used for studying many lipid bilayer membranes.[60–62] Therefore, the *r* value of DPH was measured at different concentrations above the cac for surfactant solutions at room temperature. The anisotropy is relatively higher than that of $C_{12}$Ala at concentrations just above the cac value, which increases up to a surfactant concentration of about 1.5 mM and then remains unaltered over a concentration range of 1.5−4 mM (see Figure 5). However, as the surfactant concentration increased further, the *r* value began to drop and reached a plateau at ~15 mM. The curve in Figure 5 shows an inflection at a surfactant concentration of ~5 mM. This is consistent with the decrease of the $I_1/I_3$ index at higher surfactant concentrations. A similar observation also was reported for the $C_{12}$HVal amphiphile.[45] The relatively high value of *r* in the case of the $C_{12}$HAla

(57) Miyagishi, S.; Nishida, M. *J. Colloid Interface Sci.* **1978**, *65*, 380–386.
(58) Kalyanasundaram, K.; Thomas, J. K. *J. Am. Chem. Soc.* **1977**, *99*, 2039–2044.
(59) (a) Kalyansundaram, K. *Photophysics of Microheterogeneous Systems*; Academic Press: New York, 1988. (b) Thomas, J. K. *The Chemistry of Excitation at Interfaces; ACS Monograph 181*; American Chemical Society: Washington, DC, 1984. (c) Winnik, F. M.; Regismond, S. T. A. *Colloids Surf., A* **1996**, *118*, 1–39.
(60) Shinitzky, M.; Barenholz, Y. *J. Biol. Chem.* **1974**, *249*, 2652–2657.
(61) Shinitzky, M.; Dianoux, A. C.; Itler, C.; Weber, G. *Biochemistry* **1971**, *10*, 2106–2113.
(62) Shinitzky, M.; Yuli, I. *Chem. Phys. Lipids* **1982**, *30*, 261–282.

amphiphile at low concentrations suggests an ordered environment around the DPH probe in the self-assemblies. The large value of $r$ is due to tight packing of the hydrocarbon chains and perhaps is indicative of the formation of bilayer aggregates[13,16–18] such as spherical vesicles, lamelae, or nanotubules. As discussed previously, the increase of the $r$ value with surfactant concentration corresponds to the growth of bilayer aggregates. On the other hand, the decrease of the $r$ value with the rise of [$C_{12}$HAla] above 5 mM can be attributed to the transformation of the initially formed bilayer structure to another bilayer structure such as ribbon or rod-like micelles. In fact, such a transition recently was proposed for the structurally similar $C_{12}$HVal surfactant.[45]

To further corroborate the previous results, we determined microviscosity (more appropriately, microfluidity) around the DPH probe in the surfactant aggregate. The microviscosity ($\eta_m$) can be calculated from the Debye−Stokes−Einstein relation[63]

$$\eta_m = \frac{kT}{v_h}\tau_R \quad (4)$$

where $v_h$ is the hydrodynamic volume (313 Å$^3$)[64] of the DPH probe and was estimated by the atomic increment method of Edward,[65] and $\tau_R$ is the rotational correlation time of the fluorophore and is defined by Perrin's equation as follows:[66]

$$\tau_R = \left(\frac{r_0}{r} - 1\right)^{-1}\tau_f \quad (5)$$

where $r_o$ (0.362)[67] is the steady-state fluorescence anisotropy for the DPH probe in a highly viscous solvent and $\tau_f$ is the fluorescence lifetime of the DPH molecule in the presence of surfactant. The $\tau_f$ values obtained from the analysis of fluorescence intensity decays of the DPH probe in the presence of $C_{12}$HAla and $C_{12}$Ala amphiphiles are 7.33 and 6.97 ns, respectively. A typical biexponential decay profile of DPH in $C_{12}$HAla environments is shown in Figure 3S in the Supporting Information. The microviscosity values thus calculated are presented in Table 1. The $\eta_m$ value for the self-assemblies of $C_{12}$Ala is similar to that of micellar aggregates of SDS and DTAB surfactants.[64] However, the $\eta_m$ value for the self-assemblies of $C_{12}$HAla is much larger than that of $C_{12}$Ala. The high $\eta_m$ value in the case of $C_{12}$HAla is consistent with the formation of bilayer aggregates. It should be noted that $C_{12}$Ala is structurally similar to $C_{12}$HAla without the -OH group at the 2-position. Therefore, this difference in aggregation behavior must be due to the -OH group. Perhaps, as mentioned earlier, IHBs between -OH and >NH groups of adjacent surfactant molecules in the bilayer are responsible for molecular cohesion and thus tight packing of the hydrocarbon chains of the amphiphiles in the bilayer aggregate as manifested by the $\eta_m$ value.

**Hydrogen-Bonding Interactions.** To examine as to if the IHB interaction has any role in the self-organization of $C_{12}$HAla molecules, we recorded a FT-IR spectrum (Figure 6) in $D_2O$ solvent containing 0.1 N NaOD. It can be seen that the peak (3400 cm$^{-1}$) corresponding to the O−H stretching is broad and is shifted toward lower wavenumbers. A similar broad peak at 3386 cm$^{-1}$ also was observed in the FT-IR spectrum (Figure 4S in the Supporting Information) of the solid compound. This suggests that the -OH group of the alkyl chain is hydrogen bonded. In dilute solutions where vesicles are formed, the IHB formation must be mediated through interfacial water molecules and is relatively weaker than in concentrated solution. This can be demonstrated by comparison of the stability of the aggregates upon a rise in temperature. Figure 7 shows the plot of variation of $r$ as a function of temperature for the $C_{12}$HAla surfactant at different concentrations. The $r$ value is high at low temperatures, but it decreases with a rise in temperature. The decrease of the $r$-value can be associated with the weakening of the hydrophobic interactions among hydrocarbon chains in the aggregate as a result of disruption of the intermolecular hydrogen bonds. This means that the hydrocarbon chains become more fluid at higher temperatures. In other words, a phase transition from a more ordered bilayer state to a less ordered micellar state occurs upon an increase in temperature.

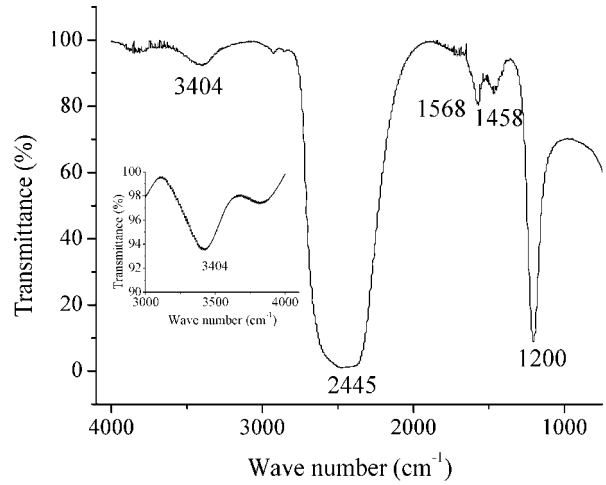


**Figure 6.** FT-IR spectrum of 50 mM $C_{12}$HAla in alkaline (0.1 N NaOD) $D_2O$ solvent; inset: H-bonded O−H region.

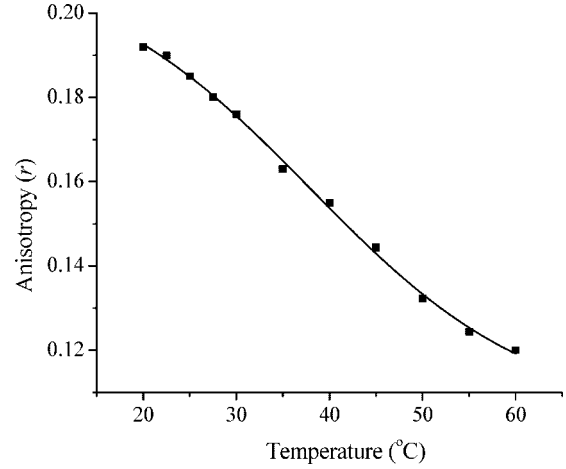


**Figure 7.** Variation of anisotropy ($r$) of DPH probe in 5 mM $C_{12}$HAla solution (20 mM phosphate buffer, pH 12.0) with temperature.

**DLS Studies.** Bilayer structures, such as vesicles, lamelae, and tubules, can be distinguished from micelles based on the size of the aggregates. The former have large sizes as compared to that of spherical micelles. Therefore, DLS was employed to determine the hydrodynamic diameter of the aggregates formed by $C_{12}$HAla and $C_{12}$Ala in the concentration range studied. The scattering intensity of $C_{12}$Ala solution even at a concentration 5 times its cac was very low, and therefore, DLS measurements were performed using a 20 mM solution. The low count for the $C_{12}$Ala surfactant at lower concentrations indicates that the aggregates present in solution are small spherical micelles that have diameters typically in the range of 3−5 nm.[68] The intensity

(63) Debye, P. *Polar Molecules*; Dover: New York, 1929.
(64) Roy, S.; Mohanty, A.; Dey, J. *Chem. Phys. Lett.* **2005**, *414*, 23–27.
(65) Edward, J. T. *J. Chem. Educ.* **1970**, *47*, 261–270.
(66) Lakowicz, J. R. *Principles of Fluorescence Spectroscopy*; Plenum Press: New York, 1983; p 132.
(67) Shinitzky, M.; Barenholz, Y. *J. Biol. Chem.* **1974**, *249*, 2652–2657.

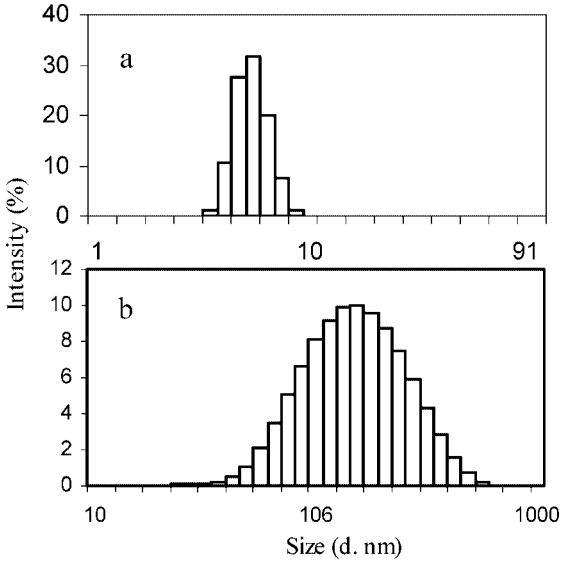


**Figure 8.** Size distributions of the aggregates in (a) 20 mM $C_{12}$Ala and (b) 0.5 mM $C_{12}$HAla surfactants.

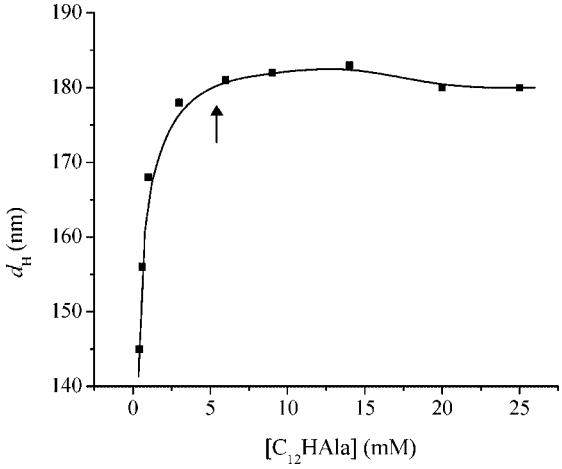


**Figure 9.** Plot of *z*-average hydrodynamic diameter ($d_H$) as a function of [$C_{12}$HAla]. The curve is a smooth line joining the experimental points.

distribution graphs of both amphiphiles are depicted in Figure 8. The size distribution in a 20 mM solution of $C_{12}$Ala is shown in Figure 8a. The *z*-average hydrodynamic diameter ($d_H$) thus obtained is ∼8 nm, suggesting the existence of ellipsoidal or cylindrical micelles, which is consistent with the lower values of $r$ and $\eta_m$ (see Table 1). Thus, it can be concluded that in dilute solutions, $C_{12}$Ala forms small spherical micelles that grow to form ellipsoidal or cylindrical micelles at higher concentrations. On the other hand, DLS measurements for $C_{12}$HAla showed the existence of large aggregates (see Figure 8b for size distribution). The *z*-average diameter is observed to be ∼145 nm. The size of the aggregates is observed to increase as shown by the plot of $d_H$ as a function of concentration (Figure 9). It is observed that the $d_H$ value initially rises, reaching a plateau above 3 mM, which suggests growth of the bilayer aggregates of the $C_{12}$HAla surfactant with concentration as also indicated by the fluorescence probe studies.

**TEM.** The TEM micrographs of negatively stained specimens prepared from aqueous $C_{12}$HAla solutions are shown in Figure 10A−E. The micrograph of the dilute solution (Figure 10A) shows the existence of large spherical vesicles having diameters in the range of 20−80 nm. This confirms the role of IHB interactions of the hydroxyl and amine moieties in the hydrocarbon chain of $C_{12}$HAla, which as discussed previously facilitates close packing of the hydrocarbon tails, leading to the formation of spherical bilayer vesicles in dilute solution. The image in Figure 10B taken for the 3 mM solution reveals a branching tubular morphology. The tubules are a few micrometers long and have an inner diameter of ∼100 nm. Formation of similar microstructures by $C_{12}$HVal already was reported by us.[45] In our earlier report, a speculation was made about the possible mechanism of formation of branching nanotubes. In fact, the generation of tubular aggregates is common in amino acid-derived surfactants.[69] However, it is interesting to see that the tubules have junctions or are connected to other tubules. Although the tubules are connected and are very long, the aqueous solutions of the amphiphiles are nonviscous, unlike solutions containing entangled worm-like micelles. Micellar branching in the case of nonionic,[70] ionic,[71–76] and mixed surfactant systems[77–80] has been reported in the literature. The branched micellar solutions were found to be nonviscous. However, the major difference between branched tubules and branched micelles is that formation of the latter follows the formation of an entangled worm-like micellar phase. On the other hand, the tubules are either formed through fusion of vesicles or by twisting of bilayer ribbons.

It appears that at a concentration greater than 5 mM $C_{12}$HAla, the tubules are transformed into flat bilayer aggregates. Clearly, the micrographs in Figure 10C,D reveal the formation of long flexible and twisted ribbons. Because the headgroup is an L-amino acid, the ribbons have a right handed twist. The width of the ribbons ranges between 25 and 50 nm. The flexible ribbons also are observed to entangle with each other to form long rope-like aggregates. The transformation of nanotubes to flat ribbon-like structures is consistent with the decrease of fluorescence anisotropy (see Figure 5) of the DPH probe. With a further increase of surfactant concentration, the entanglement of the ribbons is enhanced, and thus, they grow larger to produce thick ropes (Figure 10E) having diameters in the range of 100−200 nm. The twisting marks are clearly visible on the surface of the ropes. The ropes that are formed at a much higher concentration as expected are less flexible and more rigid structures.

**Conductivity Studies.** Because of the nature of the method involved, doubts have been cast by many researchers on the morphology of the aggregates normally observed in the negatively stained TEM micrograph. Therefore, to support the results obtained from TEM studies and to further demonstrate the formation of closed vesicles/tubules by $C_{12}$HAla, we measured

(68) Singh, M.; Trivedi, M. K.; Bellare, J. *J. Mater. Sci.* **1999**, *34*, 5315–5323.
(69) Hassan, P. A.; Raghavan, S. R.; Kaler, E. W. *Langmuir* **2002**, *18*, 2543–2548.
(70) Bernheim-Groswasser, A.; Wachtel, E.; Talmon, Y. *Langmuir* **2000**, *16*, 4131–4140.
(71) Gonzalez, Y. I.; Kaler, E. W. *Curr. Opin. Colloid Interface Sci.* **2005**, *10*, 256–260.
(72) Shashkina, J. A.; Philoppova, O. E.; Zaroslov, Y. D.; Khokhlov, A. R.; Pryikhina, T. A.; Blagodatskikh, I. V. *Langmuir* **2005**, *21*, 1524–1530.
(73) Flood, C.; Dreiss, C. A.; Croce, V.; Cosgrove, T.; Karlsson, G. *Langmuir* **2005**, *21*, 7646–7652.
(74) Schubert, B. A.; Kaler, E. W.; Wagner, N. J. *Langmuir* **2003**, *19*, 4079–4089.
(75) Raghavan, S. R.; Edlund, H.; Kaler, E. W. *Langmuir* **2002**, *18*, 1056–1064.
(76) Bernheim-Groswasser, A.; Zana, R.; Talmon, Y. *J. Phys. Chem. B* **2000**, *104*, 4005–4009.
(77) Bernheim-Groswasser, A.; Zana, R.; Talmon, Y. *J. Phys. Chem. B* **2000**, *104*, 12192–12201.
(78) Koehler, R. D.; Raghavan, S. R.; Kaler, E. W. *J. Phys. Chem. B* **2000**, *104*, 11035–11044.
(79) Kwon, S. Y.; Kim, M. W. *Phys. Rev. Lett.* **2002**, *89*, 258302–258304.
(80) Porte, G.; Gomati, R.; El Haitami, O.; Appell, J.; Marignan, J. *J. Phys. Chem.* **1986**, *90*, 5746–5751.

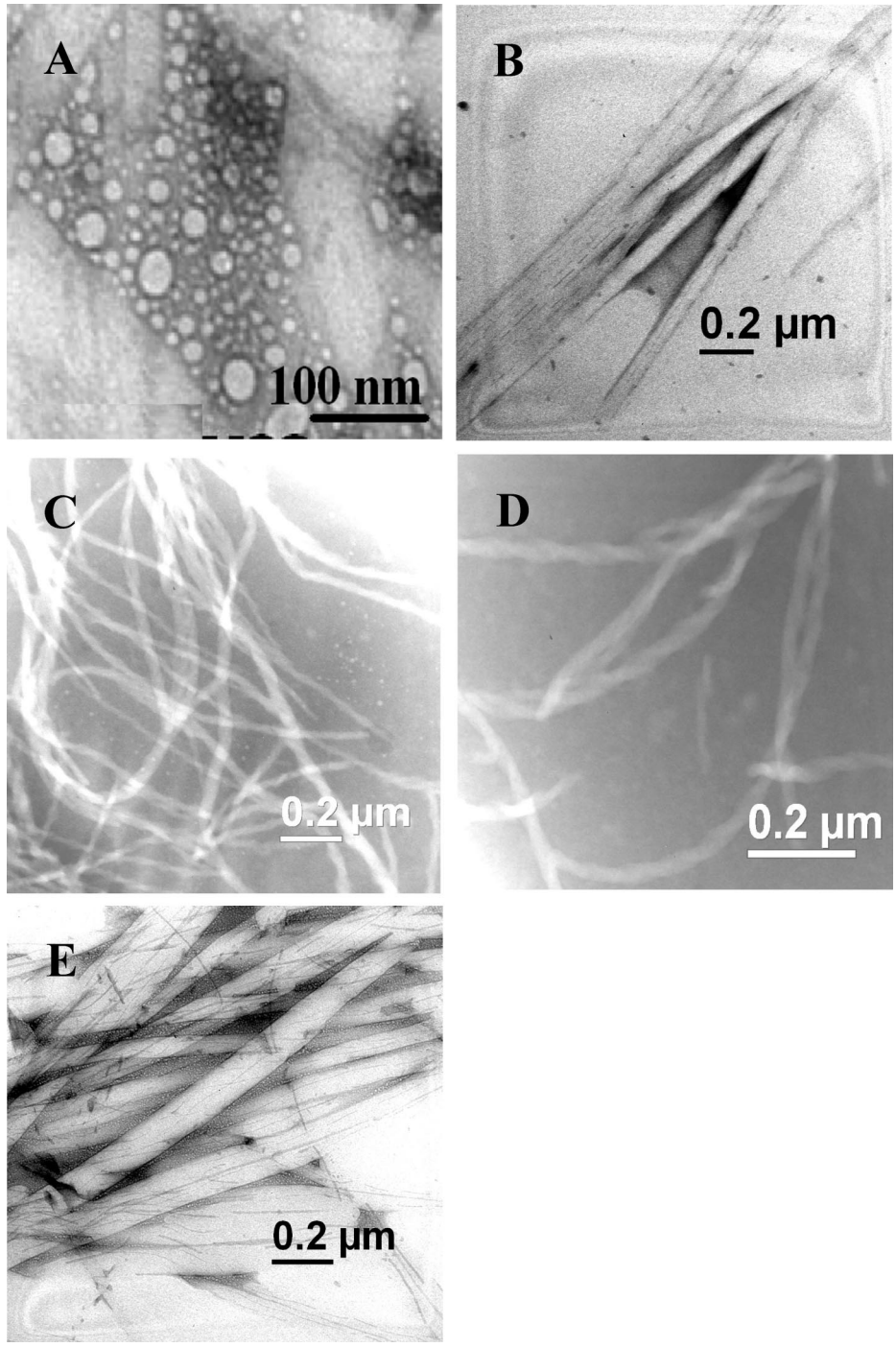


**Figure 10.** TEM images (negatively stained with aqueous 1.5% phosphotungstate, pH 12) of (A) 0.6 mM, (B) 3.0 mM, (C and D) 6 mM, and (E) 15 mM $C_{12}$HAla in 20 mM phosphate buffer (pH 12).

the conductivity of 5 mM KCl in the presence of different concentrations of surfactant at 30 °C. Bilayer aggregates, such as vesicles, entrap a part of the water and the salt present in it. Consequently, the entrapped charge carrier ions are prevented from contributing to the conductivity of the solution, which means a decrease in the conductivity of the vesicular solution. In fact, a decrease in electrical conductivity of the salt solution upon the addition of vesicle-forming surfactants has been reported in the literature.[13,81,82] It was observed that the sum of the conductivities of the solutions of 5 mM KCl and 1 mM $C_{12}$HAla (20 mM phosphate buffer) was greater than that of 1 mM $C_{12}$HAla (20 mM phosphate buffer) containing 5 mM KCl. This means that the conductivity of the KCl solution decreased in the presence of 1 mM (>$cac_1$) $C_{12}$Ala. In contrast, no significant decrease of conductivity of the KCl solution was observed in the presence of the $C_{12}$Ala surfactant. The variation of conductivity change ($\Delta\kappa$) with the increase of [$C_{12}$HAla] is shown in Figure 10. Although the initial value of $\Delta\kappa$ is small, it increases nonlinearly with surfactant concentration. The $\Delta\kappa$ value reaches a maximum at ~2 mM and then drops down at [$C_{12}$HAla] > 4 mM. It is interesting to observe that the feature of the curve is very similar to the plot in Figure 4. A similar observation also was made in the case of $C_{12}$HVal.[45] This is clear evidence of the formation

(81) Horbaschek, K.; Hoffmann, H.; Thunig, C. *J. Colloid Interface Sci.* **1998**, *206*, 439–456.
(82) Shankar, B. V.; Patanaik, A. *Langmuir* **2007**, *23*, 3523–3529.

of vesicles or nanotubes that have an aqueous core in the concentration range between 0.1 and 4 mM. Since both size and population of vesicles/nanotubes increases with surfactant concentration, more $K^+$ and $Cl^-$ ions become trapped inside the aqueous core and hence increase the $\Delta\kappa$ value. The fall of the $\Delta\kappa$ value above 4 mM might be due to the transformation of vesicles or tubules to flat lamellar aggregates and/or rod-like micelles, which release part of the entrapped water with ions. Although the fluorescence anisotropy of the DPH probe is lower (Figure 5), the microstructures formed at the highest concentration cannot be pure rod-like micelles. If the tubes were completely converted to rod-like micelles, then the $\Delta\kappa$ value would have become zero again at the highest concentration of $C_{12}$HAla employed in this work. These observations are consistent with the TEM micrographs shown in Figure 10.

**Shape of the Aggregates.** Shapes of the spontaneously formed aggregates of surfactants also can be predicted with considerable certainty using a critical packing parameter or shape factor, $P$ ($= v/(l_c A_{min})$, where $l_c$ is the critical chain length (maximum length the chain can assume), $v$ is the volume of the hydrocarbon tail, which is assumed to be fluid and incompressible, and $A_{min}$ is the optimal headgroup area as defined by Israelachvili.[83] The model predicts the formation of spherical micelles at $P \leq 1/3$, cylindrical micelles at $1/3 \leq P \leq 1/2$, vesicles or flexible bilayers at $1/2 \leq P \leq 1$, and inverted micelles at $P > 1$. Yan et al. have shown that the $P$ value for tubes is larger than that for vesicles.[84] They found tubes in the $0.7 \leq P \leq 1$ region and vesicles in the $0.5 \leq P \leq 0.7$ region. The $v$ values of the dodecyl chain for $C_{12}$HAla (371.9 Å$^3$) and $C_{12}$Ala (358.3 Å$^3$) were estimated from the molar volume of *n*-dodecane (368 Å$^3$)[65] after correction for the -OH group and H atoms according to the atomic increment method of Edward.[65] To obtain the value of $l_c$, we first optimized the geometry of the surfactant molecule using a standard MM2 force field. The linear distance (14.02 Å) between the carbon atom linked to the >NH group and the methyl carbon at the end of the chain was taken as the critical chain length. The $P$ values (Table 1) for the aggregates of the amphiphiles were calculated by using the corresponding $A_{min}$ values obtained from ST measurements. In the case of the $C_{12}$Ala surfactant, the $P$ value was <0.5, which means that the aggregates formed by the $C_{12}$Ala surfactant have spherical shapes. This also is indicated by the large value of $d_H$ in comparison to normal spherical micelles. The $P$ value for the $C_{12}$HAla surfactant, in contrast, is >0.5, which suggests the spontaneous formation of bilayer aggregates. The accuracy of this estimation is proven by the experimental results described. Since the first break in the ST plot is not very clear, we were unable to calculate the $P$ value for the aggregates formed at concentrations below $cac_2$. But, comparison of the results to that of the $C_{12}$HVal surfactant[45] suggests that vesicle structures that are present in dilute solution at [$C_{12}$HAla] < $cac_2$ are spontaneously converted to tubes upon an increase in concentration. This is in agreement with the results of ST, fluorescence probe, and TEM studies.

## Conclusion

We studied the effects of including a hydroxyl group in the hydrocarbon tail of an anionic surfactant. Accordingly, two *N*-alkyl amino acid-derived surfactants ($C_{12}$HAla and $C_{12}$Ala) were synthesized, and their aggregation behavior was studied in aqueous solutions at pH 12. We wanted to find out as to what effects the hydrogen bonding ability of the -OH group may have on the shape of the aggregates that are formed by $C_{12}$HAla. The aggregation behavior of the hydroxyl-containing surfactant $C_{12}$HAla was compared to that of a $C_{12}$Ala surfactant of similar size. The lower values of cac and $\gamma_{cac}$ indicated that the former amphiphile is more surface active than the latter. This also was suggested by the higher $pC_{20}$ and $cac/C_{20}$ values.

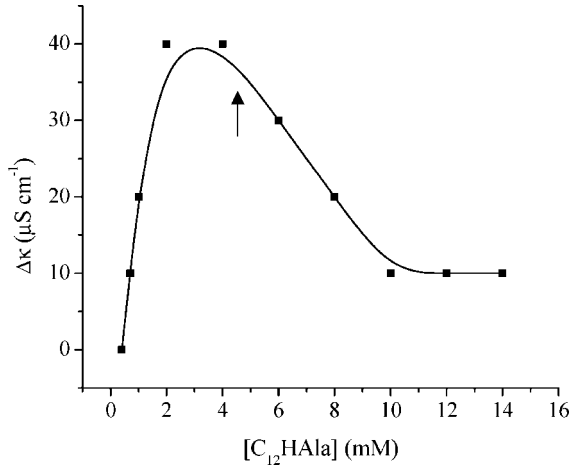


**Figure 11.** Characteristic specific conductance change ($\Delta\kappa$) with [$C_{12}$HAla] in the presence of 5 mM KCl in 20 mM phosphate buffer (pH 12.0) at 30 °C. The curve is a smooth line joining the experimental points.

From the lower cac value of the $C_{12}$HAla surfactant, it could be concluded that intermolecular hydrogen-bonding interactions (through the OH and NH groups) strengthen the hydrophobic interactions between hydrocarbon chains of adjacent surfactant molecules, thus facilitating the formation of aggregates. It appears that the hydroxyl-containing surfactant $C_{12}$HAla spontaneously forms bilayer aggregates within the whole concentration range investigated. This is consistent with the results of fluorescence anisotropy, DLS, and TEM measurements. However, $C_{12}$Ala formed normal micelles under similar conditions. In dilute solutions, the $C_{12}$HAla surfactant forms closed vesicles that are converted to tubules with an increase in concentration. The tubules in turn are converted to flexible and twisted ribbons at a surfactant concentration greater than 4 mM. The flexible ribbons are then transformed into thick and rigid rope-like aggregates. A comparison of the aggregation behavior of $C_{12}$HAla to that of $C_{12}$Ala and FT-IR spectra suggested that intermolecular hydrogen-bonding interactions are responsible for tighter packing of the hydrocarbon chains in the bilayer aggregates of the amphiphiles and hence the formation of tubules. The tubules thus formed are stable above room temperature. The microenvironments of the bilayer aggregates of $C_{12}$HAla are more polar and viscous as compared to those of micelles formed by the $C_{12}$Ala surfactant.

**Acknowledgment.** This work was financially supported by the CSIR (Grant 01(2008)/05/EMR-II), New Delhi. A.G. thanks CSIR for a research fellowship (09/081(0542)/2005-EMR-I). The authors gratefully acknowledge Dr. S. Dey, Department of Chemical Engineering, IIT, Kharagpur and Dr. N. Chattopadhyay, Jadavpur University, Kolkata for their assistance with the DLS and fluorescence lifetime measurements, respectively.

**Supporting Information Available:** Experimental details giving chemical identifications of amphiphiles, potentiometric and fluorescence titration curves, representative fluorescence intensity decay, and FT-IR spectrum. This material is available free of charge via the Internet at http://pubs.acs.org.

LA800232X

(83) Israelachvili, J. N. *Intermolecular and Surface Forces*, 2nd ed.; Academic Press: New York, 1991.

(84) Yan, Y.; Xiong, W.; Li, X.; Lu, T.; Huang, J.; Li, Z.; Fu, H. *J. Phys. Chem. B* **2007**, *111*, 2225–2230.